0022-3530/89 $3.00

Petrology of Biotite–Cordierite–Garnet Gneiss of the McCullough Range, Nevada II. P–T–a_{H_2O} Path and Growth of Cordierite During Late Stages of Low-P Granulite-Grade Metamorphism

by EDWARD D. YOUNG

Department of Geological Sciences, University of Southern California, Los Angeles, California 90089-0740

(*Received 10 February 1987; revised typescripts accepted 29 July 1988*)

ABSTRACT

Thermodynamic calculations based on addition of mass balance equations to the Gibbs Method (Spear, 1986) are used to model the cordierite-producing reaction in pelitic gneiss from the McCullough Range, southern Nevada. Calculations which treat the model paragenesis as a system open to transfer of H_2O are consistent with textural relations. Results indicate that cordierite grew by the continuous net-transfer reaction:

$$\begin{aligned} 0{\cdot}76\,\mathrm{BIO} + 1{\cdot}72\,\mathrm{SILL} + 3{\cdot}55\,\mathrm{QTZ} + 0{\cdot}27\,\mathrm{PLG} + 0{\cdot}005\,\mathrm{GRT} \\ + 0{\cdot}06\,\mathrm{Al_2R^{2+}_{-1}Si_{-1}[BIO]} \rightleftharpoons 1{\cdot}00\,\mathrm{CRD} + 1{\cdot}02\,\mathrm{KSP} + 0{\cdot}76\,\mathrm{H_2O} \\ + 0{\cdot}30\,\mathrm{FeMg_{-1}[CRD]} + 0.15\,\mathrm{FeMg_{-1}[BIO]} + 0{\cdot}0005\,\mathrm{FeMg_{-1}[GRT]} \\ + 0{\cdot}005\,\mathrm{CaNaAl_{-1}Si_{-1}[PLG]} \end{aligned}$$

with decreasing P, decreasing T, and increasing a_{H_2O}. The steep retrograde dP/dT path for these low-pressure granulites contrasts with isobaric cooling paths typical of higher pressure granulites, and suggests uplift and erosion were active during Proterozoic granulite-grade metamorphism in this area.

INTRODUCTION

The importance of continuous net-transfer reactions, which affect changes in mineral compositions and modal abundances during metamorphism, has been emphasized by Loomis (1975) and Thompson (1976). Characterization of these important reactions has historically relied upon interpretation of topologies of simplified projections. More recently, several workers have utilized quantitative approaches to study changes in mode during metamorphism (Rice & Ferry, 1982; Thompson, 1982; Thompson *et al.*, 1982; Chamberlain, 1986). Korzhinskii (1959) illustrated the advantages of considering both the intensive and extensive factors of state of a simple thermodynamic system. Full understanding of the effects of continuous net-transfer reactions requires examination of both types of variables in concert.

In this paper, the evolution of independent intensive variables and changes in mode during the later stages of granulite grade metamorphism of a pelitic gneiss are examined. The gneiss is part of a Proterozoic low-pressure granulite complex exposed in the McCullough Range of southern Nevada. The petrology of these rocks is summarized in a companion paper (Part I, Young *et al.*, 1989). The method proposed by Spear (1986) is used here to

demonstrate quantitatively that cordierite in the pelitic gneiss grew by a reaction involving consumption of biotite, sillimanite, quartz, and plagioclase, and growth of K-feldspar. It is further shown that the cordierite-producing reaction progressed with a substantial decrease in pressure, a small decrease in temperature, and an increase in activity of H_2O. These results are consistent with textural evidence and published experimental data, and illustrate the usefulness of this approach for interpreting parageneses related by continuous net-transfer reactions. The derived P–T path lends a constraint on possible causes for the Proterozoic low-pressure granulite grade metamorphic event recorded by these rocks.

PELITIC GNEISS PARAGENESES

The pelitic gneisses contain the assemblage K-feldspar + plagioclase + quartz + biotite + garnet + cordierite + sillimanite + ilmenite + hercynite + graphite. The petrology and conditions of metamorphism are described in Part I. In brief, mineral based geothermobarometry yields temperatures of 590–750 °C and pressures of ~3 to 4 kb. Mineral equilibria record low f_{O_2} ($\leq$QFM) and a_{H_2O} ($\leq$0·26) during at least the later stages of metamorphism.

Cores of cordierites poikilitically enclosing biotite and lesser garnet, together with those inclusions, comprise part of a paragenesis in these rocks distinct from that defined by other matrix grains, including cordierite oikocryst rims. The inclusions of biotite ± garnet within cordierite are significantly more magnesian than matrix grains. Biotites enclosed in cordierite also have higher Al concentrations relative to matrix biotites. Zoning in cordierites devoid of ferromagnesian silicate inclusions is characterized by relatively flat compositional gradients presumably attributable to partial homogenization by efficient volume diffusion at high temperatures (Tracy *et al.*, 1976; Woodsworth, 1977; Grew, 1981; Tracy & Dietsh, 1982; Indares & Martignole, 1984; Schreurs & Westra, 1986). In contrast, cordierite oikocrysts exhibit pronounced zoning characterized by significantly higher Mg/(Mg + Fe) in cores near inclusions of biotite ± garnet (Fig. 1). The magnesium-rich composition of the inclusions and adjacent host cordierite (hereafter referred to as inclusion assemblages) cannot be attributed to cation exchange in that they alone comprise the major ferromagnesian silicates. Moreover, an increase in Mg/(Mg + Fe) in all three phases is inconsistent with retrograde cation exchange (cf. Tracy *et al.*, 1976; Schreurs & Westra, 1986). These compositions must be related to cordierite rim and matrix grain compositions (hereafter referred to as matrix assemblages) by a continuous net-transfer reaction. Although the shape of zoning profiles in cordierite oikocrysts may have been modified by diffusion, the change in composition from the inclusion assemblages to the matrix assemblages is a vestige of zoning incurred during this reaction. Inclusion assemblages reflect conditions which prevailed during the early stages of cordierite growth. Matrix assemblages record conditions attained after crystallization of cordierite was complete. The differences in compositions of phases in these two parageneses are used to deduce the variations in P, T, a_{H_2O}, and modal abundances of minerals which occurred during cordierite growth.

METHOD

Theory

The Gibbs Method (Spear *et al.*, 1982) is a thermodynamic formulism permitting changes in mineral compositions to be related to corresponding variations in intensive factors of state. The method involves solving a system of linear differential equations, yielding useful partial derivatives. Spear (1986) has shown that the addition of mass-balance equations to

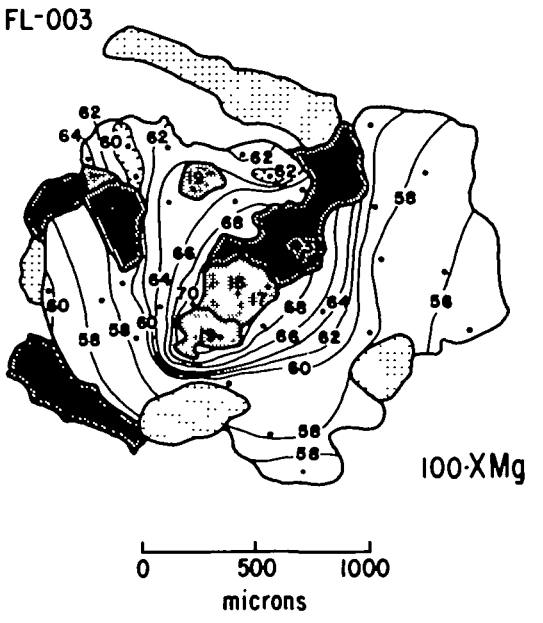

FIG. 1. Contour map of 100·0(Mg/(Mg + Fe)) for cordierite enclosing biotite (lined pattern) and garnet (fine stipled pattern). Note abrupt increase in x_{Mg} near inclusions. Solid dots indicate microprobe analysis points. Mg/(Mg + Fe) of included grains also shown. Coarse stipled pattern represents quartz.

the Gibbs Method can be used to solve simultaneously for changes in intensive and extensive variables. A useful aspect of this approach is that the total number of independent factors required to specify the state of the system may be less than that predicted by the Gibbs phase rule.

For example, the total number of independent factors, both intensive and extensive, which govern the state of a simple thermodynamic system is $C+2$ (Korzhinskii, 1959). When considering the number of intensive degrees of freedom using the Gibbs phase rule, the inherent assumption is that the number of extensive factors of state is equal to the number of phases P. This is the minimum number of extensive factors required to define the state of the system. However, in a closed system there are C constant extensive factors, one for each independent system component, leaving only 2 independent factors. The foregoing conclusion is a restatement of Duhem's Theorem.

In order to incorporate extensive variables, including the amounts of each phase M_k and amounts of each system component n_i, C mass balance equations of the form:

$$0=\sum_k\left[\sum_{j=1}^{J_k-1}(x_{k,j}v_{k,j,i})+v_{k,J_k,i}-\sum_{j=1}^{J_k-1}(x_{k,j}v_{k,J_k,i})\right]\mathrm{d}M_k \qquad (1)$$
$$+\sum_k\sum_{j=1}^{J_k-1}[M_k(v_{k,j,i}-v_{k,J_k,i})]\,\mathrm{d}x_{k,j}-\mathrm{d}n_i$$

are added to the system of equations relating intensive variables. Equation (1) is a slightly modified version of that found in Spear (1986). The $\mathrm{d}x_{k,j}$ terms are already present in the Gibbs formulation and serve to link the mass balance equations with the thermodynamic equations. The system of equations involving only intensive parameters has $C-P+2$ degrees of freedom (see Spear *et al.*, 1982), yet addition of $P+C$ extensive variables and C

equations with the form of equation (1) yields:

$$F_{tot} = (C - P + 2) + (P + C - C) = C + 2$$

or $C+2$ total degrees of freedom. The resulting set of equations permits description of the variations in state of the thermodynamic system in terms of both intensive and extensive variables. For each constant system component i, $dn_i = 0$ so that a system closed to transfer of all system components yields a variance of 2, consistent with Duhem's Theorem.

Model

The biotite–cordierite–garnet pelitic gneiss is modeled in the system K_2O–Na_2O–CaO–FeO–MgO–MnO–Al_2O_3–SiO_2–H_2O (KNCFMMASH). The phases, phase components, and required thermochemical data are given in Table 2. The compositions of phases comprising the inclusion and matrix assemblages used in the calculations are given in Table 3.

Cordierite in the pelitic gneiss contains negligible channel-filling fluid (Part I), allowing cordierite to be treated as an anhydrous phase. Preserved phase compositions are not consistent with equilibration with a silicate melt (Part I); thus the present calculations do not include melt as a stable phase. A fluid phase is also excluded, based on the fluid-absent conditions documented in Part I. Finally, hercynite is not included in the model because it is not found in textural equilibrium with the other phases, occurring exclusively as inclusions in cordierite.

Mixing-on-sites models are used to calculate $\Delta\hat{G}^k_{mix}$ and $\Delta\hat{S}^k_{mix}$ for phases k. Because the compositional variables are end member phase components j, transformation from site-specific cation mole fractions $x_{s,c}$ to end member mole fractions $x_{k,j}$ is required to calculate the Gibbs function curvature and cross-curvature terms $(\partial^2\hat{G}^k/\partial x^2_{k,j})_{T,P,x_k}$ and $(\partial^2\hat{G}^k/\partial x_{k,j}\partial x_{k,l})_{T,P,x_k}$, respectively (see Spear *et al.*, 1982 for explanation of curvature terms). The required partial second derivatives are calculated from the expression

$$\left(\frac{\partial^2\hat{G}^k}{\partial x^2_{k,j}}\right)_{T,P,x_k} = \sum_s \sum_c \left[\left(\frac{\partial^2\hat{G}^k}{\partial x^2_{s,c}}\right)\left(\frac{\partial x_{s,c}}{\partial x_{k,j}}\right) + \sum_d \left(\frac{\partial^2\hat{G}^k}{\partial x_{s,c}\partial x_{s,d}}\right) \times \left(\frac{\partial x_{s,c}}{\partial x_{k,j}}\right)\left(\frac{\partial x_{s,d}}{\partial x_{k,j}}\right) + \left(\frac{\partial^2 x_{s,c}}{\partial x^2_{k,j}}\right)\left(\frac{\partial\hat{G}^k}{\partial x_{s,c}}\right)\right] \quad (2)$$

for curvatures, and

$$\left(\frac{\partial^2\hat{G}^k}{\partial x_{k,j}\partial x_{k,l}}\right)_{T,P,x_k} = \sum_s \sum_c \left[\left(\frac{\partial^2\hat{G}^k}{\partial x^2_{s,c}}\right)\left(\frac{\partial x_{s,c}}{\partial x_{k,j}}\right)\left(\frac{\partial x_{s,c}}{\partial x_{k,l}}\right) + \sum_d \left(\frac{\partial^2\hat{G}^k}{\partial x_{s,c}\partial x_{s,d}}\right)\left(\frac{\partial x_{s,c}}{\partial x_{k,j}}\right)\left(\frac{\partial x_{s,d}}{\partial x_{k,l}}\right) + \left(\frac{\partial^2 x_{s,c}}{\partial x_{k,j}\partial x_{k,l}}\right)\left(\frac{\partial\hat{G}^k}{\partial x_{s,c}}\right)\right] \quad (3)$$

for cross-curvatures, where j and l designate independent end members. The $(\partial x_{s,c}/\partial x_{k,j})$ terms are the elements of the Jacobian matrix used to transform the $x_{s,c}$ to $x_{k,j}$. In the cases where mixing occurs on only one site (e.g., garnet), equations (2) and (3) reduce to the forms given by Spear & Selverstone (1983).

To construct the set of equations comprising the model system, a starting point consisting of initial phase compositions and abundances, and a corresponding initial T and P must be chosen. The matrix assemblage (Table 3) was chosen as the starting point for these

TABLE 1

List of symbols

M_k	moles of phase k
n_i	moles of system component i
$x_{k,j}$	mole fraction of phase component j in phase k
$x_{k,l}$	mole fraction of phase component l in phase k
$x_{s,c}$	mole fraction of cation c on crystallographic site s
$x_{s,d}$	mole fraction of cation d on site s
J_k	total number of phase components for phase k
$v_{k,j,i}$	moles of system component i in phase component j for phase k
$v_{k,J_k,i}$	as above for dependent system component J_k
$^\circ$	superscript signifying pure phase at P and T
$\hat{G}^k$	molar Gibbs free energy for phase k
$\Delta\hat{G}^k_{mix}$	Gibbs free energy of mixing for phase k
$\Delta\hat{S}^k_{mix}$	entropy of mixing for phase k
$\hat{S}^\circ_{298}$	molar third law entropy for pure substance at 298·15 K, J mol^{-1} K^{-1}
$\hat{V}^\circ_{1b,298}$	molar volume for pure substance at 1 b and 298·15 K, J b^{-1}
R	Gas constant
$f^{P,T}_{H_2O}$	fugacity of H_2O at P and T, bars

TABLE 2

Phases, phase components, and thermochemical data for model

Phases	*Components*	*Abbreviations*	$\hat{S}^\circ_{298}$ *J/K-mol*	$\hat{V}^\circ_{1b,298}$ *J/b-mol*
garnet (GRT)	$Mg_3Al_2Si_3O_{12}$	py	260·76	11·327[1]
...	$Fe_3Al_2Si_3O_{12}$	alm	316·31	11·528[2]
...	$Ca_3Al_2Si_3O_{12}$	gros	255·50	12·530[1]
...	$Mn_3Al_2Si_3O_{12}$	spes	311·71	11·791[2]
cordierite (CRD)	$Mg_2Al_3Si_5AlO_{18}$	Mg-crd	407·20	23·322[1]
...	$Fe_3Al_3Si_5AlO_{18}$	Fe-crd	466·75	23·707[3]
biotite (BIO)	$KMg_3AlSi_3O_{10}(OH)_2$	phl	319.66	14.991[1]
...	$KFe_3AlSi_3O_{10}(OH)_2$	ann	397.90	15·432[2]
...	$KMn_3AlSi_3O_{10}(OH)_2$	Mnb	420·49	15·921[2]
...	$KFe_2AlAl_2Si_2O_{10}(OH)_2$	Al-ann	469.22	17·776[4]
plagioclase (PLG)	$NaAlSi_3O_8$	abp	207·40	10·007[1]
...	$CaAl_2Si_2O_8$	an	199·30	10·079[1]
K-feldspar (KSP)	$KAlSi_3O_8$	or	214·20	10·872[1]
...	$NaAlSi_3O_8$	abk	207·40	10·007[1]
sillimanite (SILL)	Al_2SiO_5	sill	96·11	4·990[1]
quartz (QTZ)	SiO_2	qtz	41·46	2·269[1]

1. Robie *et al.* (1978).
2. Spear & Selverstone (1983).
3. Holdaway & Lee (1977), reaction 5.
4. Calculated from data of Robie *et al.* (1978).

calculations. In other words, the *final state* of the system has been used to provide the *initial conditions* for the model.

Starting compositions for biotite, garnet, plagioclase, and K-feldspar were taken from rims of matrix grains near the poikilitic cordierite shown in Fig. 1. The rim of the cordierite oikocryst in Fig. 1 was used as the initial cordierite composition. The cordierite-garnet thermobarometer of Martignole & Sisi (1981) yields a temperature of 670 °C and a pressure of 3·2 kb for this assemblage, serving as the starting T and P, respectively. A norm calculated from a whole-rock analysis of the pelitic gneiss provided an initial estimate of the modal

TABLE 3

Mineral compositions for model in cations per formula unit

	Matrix assemblage					*Inclusion assemblage**		
	BIO	*GRT*	*CRD*	*PLG*	*KSP*	*BIO*	*GRT*	*CRD*
Si	2·671	3·092	5·020	2·699	2·979	2·696	2·940	4·872
Al	1·562	1·869	3·975	1·310	1·024	1·721	2·035	4·116
Al^{VI}	0·233	—	—	—	—	0·417	—	—
Al^{IV}	1·329	—	—	—	—	1·304	—	—
Fe_{tot}	1·277	2·340	0·802	—	—	1·105	2·292	0·576
Mn	0·001	0·118	—	—	—	0·003	0·081	—
Mg	1·109	0·469	1·188	—	—	1·304	0·584	1·490
Ca	0·002	0·084	—	0·291	0·009	0·001	0·097	—
Na	0·018	—	—	0·678	0·250	0·023	—	—
K	0·956	—	—	0·009	0·74	0·905	—	—

* Inclusion assemblage feldspar compositions calculated from model.

abundances of phases for the matrix assemblage. Calculated molar abundances were normalized to 100 moles. The initial abundance of cordierite was iteratively modified during the course of the calculations (see Results below). A more accurate estimate of the initial mode for the matrix assemblage is not required for the calculations presented below (see the discussions in the Results and Error Analysis sections).

With the exception of H_2O, the model system is assumed to be closed to exchange of system components with the surroundings. Two sets of calculations are used to account for the behaviour of H_2O. In the first, dn_{H_2O} is set equal to 0, eliminating dn_{H_2O} as a variable. These calculations depict the system as completely closed. The second set includes dn_{H_2O}, corresponding to the system open to transfer of water.

The homogeneous system of linear differential equations comprising the model is available from the author. The Gibbs phase rule indicates an intensive variance of 4 for this system. Incorporation of the extensive constraints $dn_i = 0$ reduces the *total* variance (F_{tot}) to 2 or 3, depending on the status of H_2O as a mobile or immobile component. Solutions for the system of equations permit variations in phase composition to be related to corresponding changes in factors of state. In this case, the compositions of biotite, cordierite, and garnet in the inclusion assemblage shown in Fig. 1 are used to derive the changes in T, P, μ_{H_2O}, and M_k attending growth of the cordierite oikocrysts. Microprobe analyses show that the concentration of Mn in biotite does not vary from inclusions to matrix grains. This observation is used to calculate solutions in the H_2O-open system model by setting dx^{BIO}_{Mnb} equal to zero.

Manipulations required to solve the system of equations have been described by Spear *et al.* (1982). Solution vectors for inhomogeneous, square equivalents of the matrix equation have been obtained using Gaussian elimination with partial pivoting and iterative improvement. The accuracy of the calculations is discussed in the Error Analysis section.

RESULTS

Intensive parameters

P *and* T

Calculated P–T isopleths for the mole fractions of the Fe-end member in cordierite, almandine in garnet, annite in biotite, and Al-annite in biotite are shown in Fig. 2. The slopes and spacings are identical for both the H_2O-closed and H_2O-open models. The diagram

therefore applies to both cases and serves to corroborate the validity of using constant x_{Mnb}^{BIO} in the latter. Trial numerical integration calculations show that the slopes and spacings of isopleths do not change significantly over the P–T interval of interest, and the composition isopleths are adequately represented by straight lines. Composition isopleths for the feldpsars and grossular component in garnet are not shown in Fig. 2 for clarity. It is noteworthy that the garnet and cordierite isopleths are similar to those used for thermobarometry by Martignole & Sisi (1981) and Aranovich & Podlesskii (1983).

The four independent composition parameters shown in Fig. 2 can be used to obtain the temperature and pressure of equilibration of the inclusion assemblage relative to that of the matrix assemblage. Using all four parameters, rather than the requisite two, provides a closure error which serves as a measure of internal consistency and as an ad hoc test for preservation of equilibrium compositions. The inclusion assemblage isopleths are shown as the heavy lines in Fig. 2. The cordierite and biotite isopleths yield a crossing corresponding to a temperature and pressure approximately 50 °C and 1 kb higher, respectively, than that

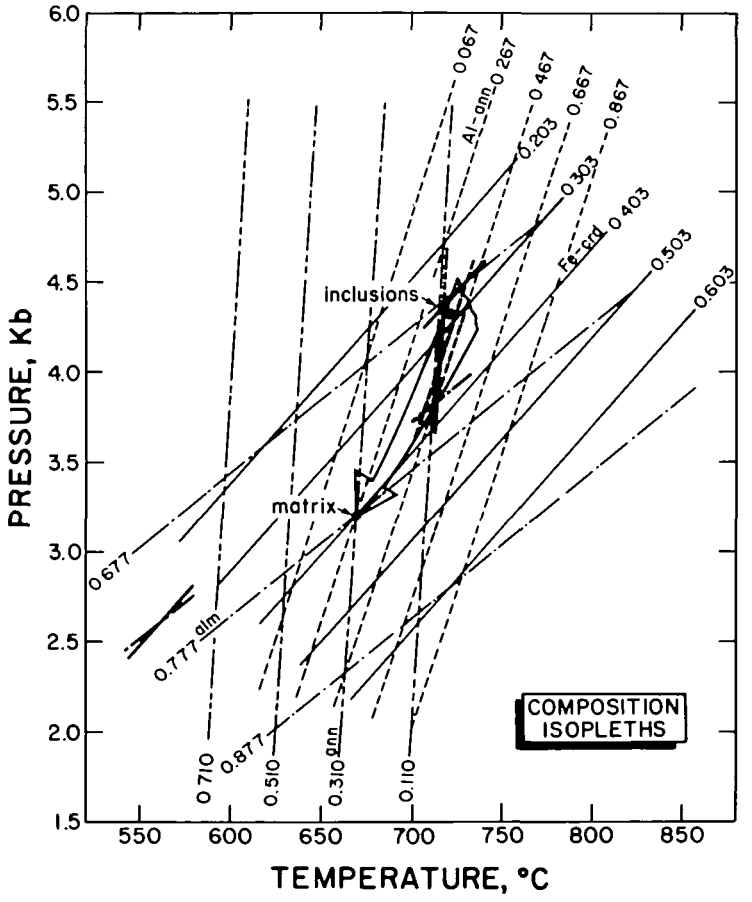

FIG. 2. P–T isopleths for x_{alm}^{GRT}, x_{ann}^{BIO}, x_{Al-ann}^{BIO}, and x_{Fe-crd}^{CRD}. Matrix assemblage is marked by the solid dot at 670° and 3·2 kb. Isopleths for inclusions and their host cordierite core are shown as heavy contours. Intersection of isopleths for cordierite oikocryst core and enclosed biotite and garnet defines P and T for the inclusion assemblage. The preferred inclusion assemblage intersection is represented by the solid dot at 720° and 4·3 kb. Arrow marks the P–T path defined by the matrix and inclusion assemblages.

of the matrix assemblage. The almandine isopleth is consistent with this higher T and P of equilibration, but lies somewhat below the intersection of the other three isopleths.

The anomalously high almandine component in the garnet inclusions can be explained by rotation of tie lines about a bulk composition lying near the composition of cordierite during retrograde resetting of $K_D^{(Mg/(Mg+Fe))}$ for garnet and cordierite. Cordierite is presently more voluminous than garnet in the assemblage being modeled (Fig. 1) by a factor of approximately 10 to 1. This requires cation exchange between the garnet inclusions and the host cordierite along the retrograde path to result in large changes in garnet composition with comparatively little change in cordierite composition. In fact, the inclusion almandine and nearby host Fe-end member cordierite isopleths also cross at a P–T point below the starting point corresponding to the matrix assemblage (Fig. 2). This low P–T point is either a spurious crossing, or represents a valid point encountered during retrogression and final equilibration. The pressure and temperature indicated by this point are consistent with reset pressures and temperatures recorded by several thermobarometers in the pelitic gneiss (Part I). Compositions of included biotites have not been significantly effected by retrograde cation exchange with their cordierite host apparently because the amounts of these phases are more comparable in the assemblage of interest, and because the temperature dependency of the distribution coefficient for these phases is apparently less than that for garnet and cordierite (Holdaway & Lee, 1977).

The high almandine component not withstanding, overall agreement between the four independent parameters in defining a P–T region in Fig. 2 is strong evidence that the inclusions and nearby host cordierite comprise an equilibrium assemblage. This assemblage is related to the matrix phase and cordierite rim compositions by a continuous net-transfer reaction involving growth of the cordierite oikocryst. The indicated dP/dT path is approximately 22 b/°C.

a_{H_2O}

In the H_2O-closed system model, the chemical potential of water (μ_{H_2O}) is buffered, varying with T and P subject to the constraints imposed by mineral equilibria. In the H_2O-open system model, μ_{H_2O} is also buffered because no fluid phase is present to impose a constant chemical potential. In both models, H_2O is therefore not a K-component as defined by Thompson (1970). The H_2O-open system calculations are seemingly at odds with the assertion of Korzhinskii (1959) that either the mass or the chemical potential of a system component must be an equilibrium factor of state. Both parameters for water are treated as variables in the open system calculations, with n_{H_2O} and μ_{H_2O} being defined by T, P, x_{Mnb}^{BIO}, and the constant moles of other system components. The H_2O-open model corresponds to conditions where H_2O diffuses at such low rates that a fluid phase is not sustained along grain boundaries (Thompson, 1983). Rumble (1982, p. 231) discussed this apparent inconsistency in the 'either/or nature' of the J- vs. K-component classification of system components.

The buffered behaviour of H_2O permits calculation of $\Delta\mu_{H_2O}$ P–T isopleths for both the H_2O-closed and H_2O-open models. The results of these calculations are shown in Fig. 3 where the matrix assemblage has arbitrarily been assigned a $\Delta\mu_{H_2O}$ of zero. In Fig. 3, the P–T path defined by the inclusion and matrix assemblages in Fig. 2 defines the attendant change in μ_{H_2O}. The exact slopes and spacings of the chemical potential isopleths are slightly different in the open and closed system calculations, but both scenarios indicate an increase in μ_{H_2O} on the order of 5 to 6 kJ/mol during growth of cordierite (Fig. 3).

A more explicit expression of the behaviour of the H_2O component with progression along the P–T path is afforded by relating the derived $\Delta\mu_{H_2O}$ to the corresponding change in

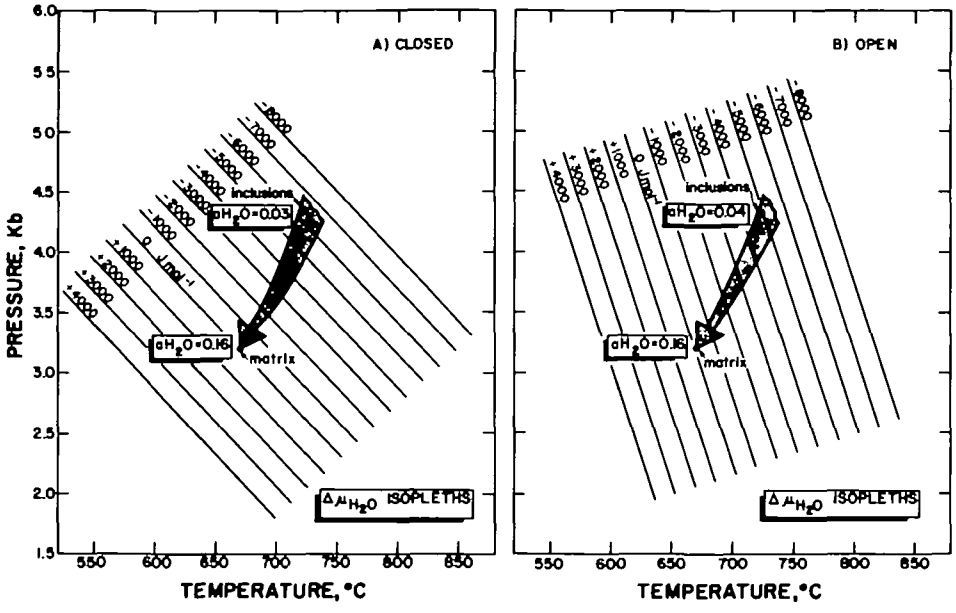

FIG. 3. P–T isopleths for $\Delta\mu_{H_2O}$ relative to the matrix assemblage in the H_2O-closed (A) and H_2O-open (B) models. P–T path from Fig. 2 defines the change in μ_{H_2O} from the inclusion assemblage to the matrix assemblage.

a_{H_2O}. The activity of H_2O for the matrix rim compositions has been calculated using the method of Phillips (1980) (Part I), yielding a mean value of 0·16 for a_{H_2O} relative to a standard state of pure H_2O vapor at P and T. The expressions

$$RT\ln a_{H_2O} = RT\ln(f^{P,T}_{H_2O}) - RT\ln(f^{\circ P,T}_{H_2O}) \quad (4)$$

$$\mu^{P,T}_{H_2O} = \mu^{0{\cdot}01,T}_{H_2O} + RT\ln(f^{\circ P,T}_{H_2O}) + RT\ln a_{H_2O} \quad (5)$$

$$\mu^{P_2,T_2}_{H_2O} - \mu^{P_1,T_1}_{H_2O} = RT_2\ln(a^{P_2,T_2}_{H_2O}) + RT_2\ln(f^{\circ P_2,T_2}_{H_2O}) - RT_1\ln(a^{P_1,T_1}_{H_2O}) - RT_1\ln(f^{\circ P_1,T_1}_{H_2O}) \quad (6)$$

and the f_{H_2O} tables of Burnham *et al.* (1969) have been used to calculate the change in a_{H_2O} from $\Delta\mu_{H_2O}$. The activities for the matrix and inclusion assemblages are shown in Fig. 3. Activities for H_2O defined by the inclusion assemblage are 0·03 and 0·04 for the H_2O-closed and H_2O-open models, respectively. Both models indicate an increase in a_{H_2O} on the order of 0·10. From equation (4) the corresponding changes in f_{H_2O} for the closed and open system models are +191 and +211 b, respectively.

Extensive parameters

Calculation of the changes in modal abundances of mineral phases accompanying progression along the P–T path shown in Fig. 2 is afforded by contouring P–T space with isopleths of constant abundance for each phase. The assumption is made that the amount of cordierite in the inclusion assemblage, representing early growth of cordierite, was exceedingly small. The assumption provides an initial condition of nearly zero moles of cordierite at the high-P high-T end of the path in Fig. 2. This initial condition does not significantly effect the final outcome (see Error Analysis below), but is preferred over the

alternative of assuming that the observed average modal proportion (or average normative quantity) of cordierite in the pelitic gneiss is appropriate for the matrix model assemblage. Use of the average mode or norm is considered to be unreliable because this value will not in general correspond to the more relevant effective modal proportion of cordierite which actually was reacting in the domain being modeled. This domain was eventually dominated by cordierite (Fig. 1), resulting in an effective abundance of cordierite much greater than the average mode for the rock. The initial condition of nearly zero cordierite for the inclusion assemblage was satisfied by iteratively adjusting the starting (matrix assemblage) moles of cordierite.

In contrast to the intensive variable calculations, the calculated variations in abundances of phases is critically dependent on the mobility of H_2O. For example, because biotite is the sole hydrous phase, its abundance must obviously be fixed if the system is treated as closed to transfer of water. A fixed amount of biotite in turn requires cordierite to grow primarily at the expense of garnet.

Textural evidence (Part I) clearly indicates that biotite, and not garnet, was a major reactant phase in the cordierite-producing reaction. This empirical constraint can only be satisfied by treating the model system as one open to transfer of H_2O. Therefore, only the H_2O-open system calculations are presented below.

Inspection of equation (1) and the coefficient matrix for the complete system of equations shows that for a linear P–T path, such as that in Fig. 2, the changes in coefficients involving M_k terms are linear and cancel, with the exception of $+2M_{BIO}$ and $-3M_{BIO}$ for $dx^{BIO}_{Al-annite}$. The result is that P–T isopleths for phase abundances can be adequately depicted as regularly spaced straight lines. Trial numerical integration calculations confirm this conclusion.

To approximate modal or volume proportions of phases, the mole unit isopleths have been converted to oxygen equivalent units normalized to 100 total oxygens. The P–T % oxygen unit isopleths for the H_2O-open model, together with the P–T path from Fig. 2, is shown in Fig. 4. Only isopleths for cordierite, biotite, garnet, and sillimanite are shown for clarity. The M_k isopleths show that cordierite grew with decreasing pressure and temperature primarily at the expense of biotite and sillimanite. It should be pointed out that using the open system model does not force biotite to be consumed. The reaction, in terms of moles of phases, along the P–T path is:

$$0{\cdot}76\,\mathrm{BIO} + 1{\cdot}72\,\mathrm{SILL} + 3{\cdot}55\,\mathrm{QTZ} + 0{\cdot}27\,\mathrm{PLG} + 0{\cdot}005\,\mathrm{GRT} \rightleftharpoons$$
$$+ 1{\cdot}00\,\mathrm{CRD} + 1{\cdot}02\,\mathrm{KSP} + 0{\cdot}76\,\mathrm{H_2O}. \qquad (7)$$

The oxygen unit proportions of phases for the matrix and inclusion assemblages are listed in Table 4. It is emphasized that the exact proportions of phases derived from this analysis are effective abundances, or amounts of phases participating in the reaction in the domain being modeled. Therefore, the proportions of phases shown in Table 4 do not necessarily reflect the average mode of the pelitic gneiss. A complete depiction of the reaction represented by equation (7) requires addition of exchange components, representing the variations in phase composition shown in Fig. 2. The complete reaction is described in mole units by the equation:

$$0{\cdot}76\,\mathrm{BIO} + 1{\cdot}72\,\mathrm{SILL} + 3{\cdot}55\,\mathrm{QTZ} + 0{\cdot}27\,\mathrm{PLG} + 0{\cdot}005\,\mathrm{GRT}$$
$$+ 0{\cdot}06\,\mathrm{Al_2R^{2+}_{-1}Si_{-1}[BIO]} \rightleftharpoons 1{\cdot}00\,\mathrm{CRD} + 1{\cdot}02\,\mathrm{KSP} + 0{\cdot}76\,\mathrm{H_2O}$$
$$+ 0{\cdot}30\,\mathrm{FeMg_{-1}[CRD]} + 0{\cdot}15\,\mathrm{FeMg_{-1}[BIO]}$$
$$+ 0{\cdot}0005\,\mathrm{FeMg_{-1}[GRT]} + 0{\cdot}005\,\mathrm{CaAlNa_{-1}Si_{-1}[PLG]}. \qquad (8)$$

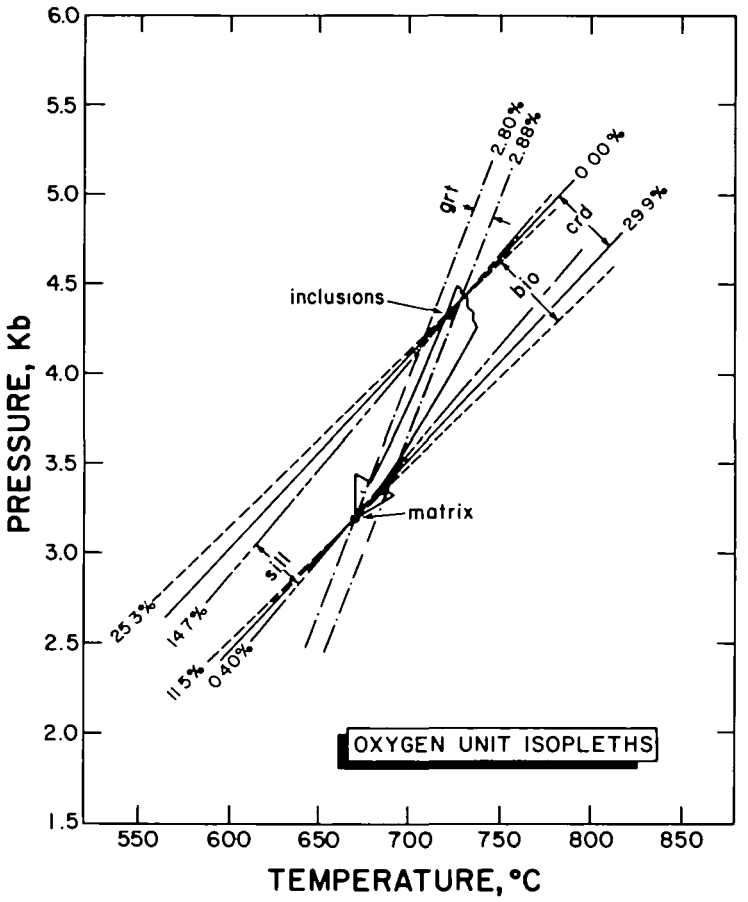

FIG. 4. *P–T* isopleths for per cent oxygen unit abundances of biotite, cordierite, garnet, and sillimanite for the H_2O-open model. *P–T* path from Fig. 2 defines the changes in phase abundances from the inclusion assemblage to the matrix assemblage.

Several petrographic features characteristic of the pelitic gneiss unit are consistent with Fig. 4. Foremost is the strict spatial association among biotite, cordierite, and sillimanite (Part I). Proximity of these phases is to be expected in light of the strong negative correlation between the amount of biotite and sillimanite, and the amount of cordierite along the calculated *P–T* path. The lack of any regular spacial relationship between garnet and cordierite is consistent with evolution along a *P–T* path nearly parallel with isopleths for modal garnet, and with the large spacing of these isopleths relative to those for the other phases. The substantial consumption of reactant sillimanite suggested by Fig. 4 is evidenced by extensive mantling of sillimanite by cordierite (Part I). Apparently, overgrowth of cordierite reduced the amount of sillimanite available for further reaction. Agreement between the textural features of the pelitic gneiss and Fig. 4 indicates that at least portions of the rock behaved as fluid-absent systems open to transfer of H_2O.

ERROR ANALYSIS

Computational uncertainties in these calculations derive from potential rounding errors attributable to the degree of ill-conditioning of the coefficient matrices, uncertainty in the

TABLE 4

Oxygen unit proportions of phases in model assemblages (%)

	Inclusion	*Matrix**
BIO	25	11
CRD	<0·1†	30
GRT	2·9	2·8
PLG	36	33
KSP	6·2	20
SILL	15	0·4
QTZ	15	2·8

* Calculated from whole rock chemistry.

† Assumed, see text.

initial estimates for effective modal abundances, and analytical errors inherent in the electron microprobe analyses.

Rounding errors have been controlled by performing iterative improvement to refine solutions until convergence to within 5 decimal points was achieved. In addition, answers obtained using Gaussian elimination were cross-checked against answers calculated from a least squares algorithm. Solutions from both methods agreed to within 4 or 5 decimal points. Minor perturbations of elements of the coefficient matrices showed no signs of instability. Calculated solutions are believed to be numerically exact to 4 or 5 decimal points.

Slopes and spacings of intensive parameter isopleths are not sensitive to the relative amounts of phases used, as shown by trial calculations and inspection of the coefficient matrix and equation (1). Slopes of isopleths for phase abundances are also insensitive to the proportions of phases, as might be predicted from equation (1). However, spacings of phase abundance isopleths are dependent upon the relative abundances of phases (Fig. 5). Once the initial relative modal abundances have been established, dependencies such as that shown in Fig. 5 cancel with progression along a linear P–T path, as described above. These dependencies are important, however, because the initial estimate for the mode influences the spacings of M_k isopleths traversed by the P–T path. The significance of this influence can be better evaluated by first establishing the uncertainty associated with isopleth spacings arising from analytical error in the mineral analyses.

A Monte Carlo routine (see Anderson, 1976) was used to propagate the uncertainties in mineral analyses (referred to as analytical errors) to all of the solutions used to construct the P–T isopleth diagrams (Figs. 2–4). Variances obtained from replicate analyses were propagated through calculations of composition and thermochemical parameters to obtain standard errors for the stochastic elements of the coefficient matrices (e.g. mol fractions, molar volumes, molar entropies, Gibbs function curvatures). Errors for solution vectors were obtained by recalculating solutions 700 times (Monte Carlo iterations) using random draws from normal parent populations for each stocastic coefficient. The large number of iterations provided stable variances for each solution.

Results show that relative uncertainties for isopleth slopes and spacings attributable to analytical errors are generally on the order of $\pm 5\%$ to $\pm 35\%$ at the 68% confidence level (Table 5). These uncertainties substantially reduce the need to determine accurately the effective mode of the initial (matrix) assemblage when deriving modal isopleth spacings (Fig. 5).

The uncertainties in isopleth slopes and spacings stemming from analytical errors are not large enough to affect changes in topologies of P–T contours (e.g., Figs. 2–4), and therefore

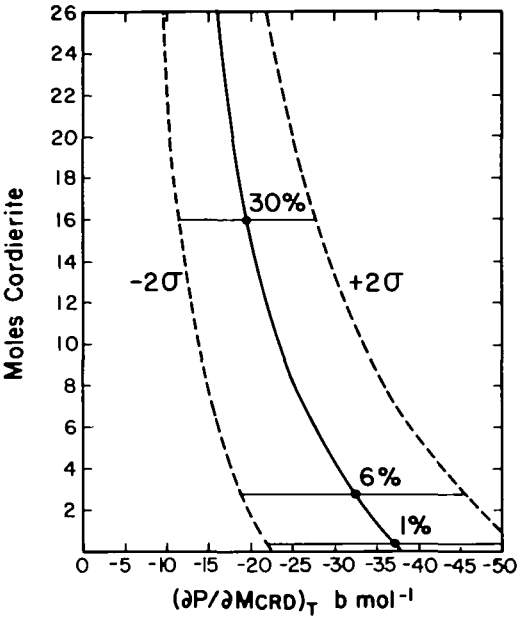

FIG. 5. Plot of isopleth spacing for abundance of cordierite in mole units ($(\partial P/\partial M_{CRD})_T$) vs. moles of cordierite (M_{CRD}) with all other amounts of phases fixed. Dashed lines represent 1σ uncertainty in spacing from Monte Carlo analysis. Solid dots mark the proportions of cordierite in oxygen units corresponding to indicated moles.

TABLE 5

Examples of partial derivatives for P–T *isopleth slopes and spacings and their* 1σ *uncertainties from Monte Carlo analysis*

Parameter	*Mean*	*Uncertainty*
$(\partial T/\partial P)_{x_{Al-ann}}$	0·032	±4·1%
$(\partial T/\partial x_{Al-ann})_P$	113·0	±5·8%
$(\partial T/\partial P)_{x_{alm}}$	0·124	±15%
$(\partial T/\partial x_{alm})_P$	1051	±27%
$(\partial T/\partial P)_{x_{Fe-crd}}$	0·089	±34%
$(\partial T/\partial x_{Fe-crd})_P$	440·0	±54%
$(\partial P/\partial T)_{M_{CRD}}$	10·88	±13%
$(\partial P/\partial M_{CRD})_T$	−35·75	±21%
$(\partial P/\partial T)_{M_{BIO}}$	10·31	±17%
$(\partial P/\partial M_{BIO})_T$	51·36	±14%

do not obviate the fundamental conclusions of the Gibbs Method analysis. They are sufficient, however, to demand consideration when deriving exact quantities for the magnitude of changes in intensive and extensive parameters. Similar effects of microprobe analytical error on calculated P–T paths have been reported by Spear & Rumble (1986). To illustrate the effects of analytical error, the P–T regions defined by 1σ errors in cordierite and biotite composition isopleths for the inclusion assemblage, their zone of intersection, and the P–T path from Fig. 2 are shown in Fig. 6. The figure shows that the steeply positive slope of the P–T path is not altered by the analytical errors, but absolute values for ΔP and ΔT are sensitive to these uncertainties. With the exception of garnet, analogous plots for extensive

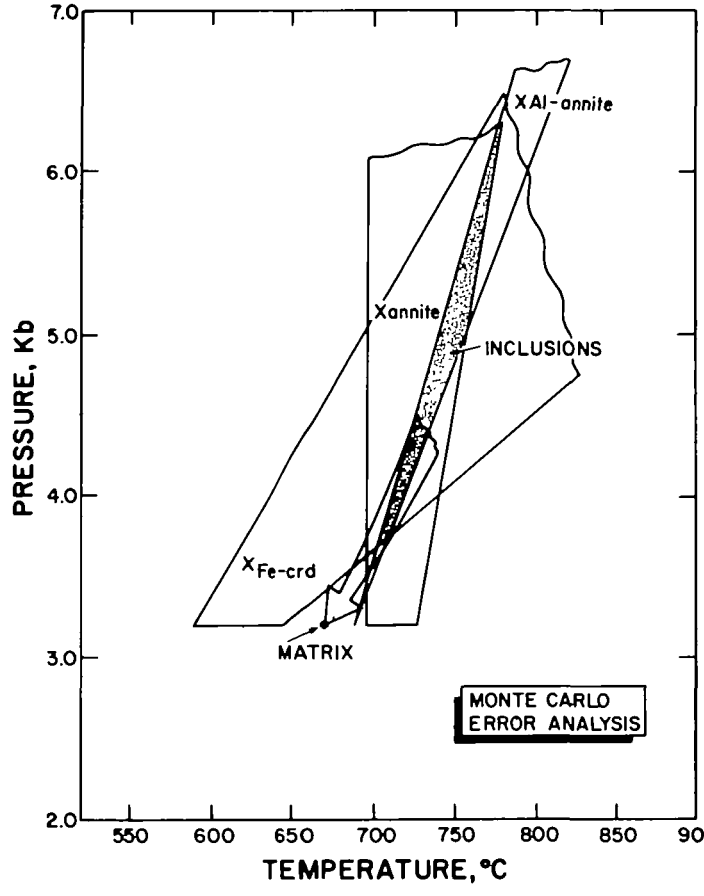

FIG. 6. P–T plot showing fields defined by 1σ uncertainties from Monte Carlo analysis for inclusion assemblage x^{BIO}_{ann}, x^{BIO}_{Al-ann}, and x^{CRD}_{Fe-crd} isopleths. Shaded overlap of fields illustrates uncertainty in P–T location of the inclusion assemblage. P–T path from Fig. 2 is shown for comparison.

parameters similarly show that relative changes in phase abundances are preserved, but magnitudes of changes in mode vary. The uncertainty in the P–T isopleths for modal abundance of garnet is large enough that their slopes in Fig. 4 are questionable. As a result, exceedingly small quantities of garnet may appear on either side of equation (8) with commensurably small changes in the coefficients for plagioclase.

DISCUSSION

Growth of cordierite

Cordierite coexisting with biotite + K-feldspar + sillimanite ± garnet comprises the zone corresponding to the highest grade in some regionally metamorphosed terranes (e.g., Reinhardt, 1968; Hollister, 1977; Jamieson, 1984; Schreurs & Westra, 1986), suggesting that where biotite and sillimanite are important reactant phases, cordierite is stabilized by prograde reactions. Experimental studies (Hoffer, 1976; Holdaway & Lee, 1977) confirm that formation of cordierite at the expense of biotite and sillimanite is favored by increasing temperature at *constant* pressure. In view of these data, one might question the feasibility of

growth of cordierite with decreasing T in this assemblage. It will be shown that the model presented here is not in conflict with the existing body of data pertaining to the stability of cordierite in pelitic rocks.

As pointed out by A. B. Thompson (1983), interpretations of multiple parageneses related to one another by dehydration reactions are often unduly influenced by consideration of temperature alone (i.e. prograde vs. retrograde). The variable P–T trajectories of metamorphic paths shows that pressure is an equally important factor of state. Comparison of the results presented here with the experimentally derived P–T relations presented by Holdaway & Lee (1977) serves to illustrate this point.

The steeply positive slope for the univariant reaction:

$$\mathrm{BIO} + \mathrm{SILL} + \mathrm{QTZ} \rightleftharpoons \mathrm{CRD} + \mathrm{GRT} + \mathrm{KSP} + \mathrm{H_2O}$$

in the system K_2O–FeO–MgO–Al_2O_3–SiO_2–H_2O (KFMASH) at $P_{H_2O} = 0{\cdot}4\ P_{total}$ shown by Holdaway & Lee (1977) is reproduced in Fig. 7. A clockwise prograde metamorphic P–T path at moderate pressures would intersect this univariancy, resulting in initial growth of small amounts of cordierite at the expense of biotite, sillimanite, and quartz. Subsequent decreases in pressure and temperature brought about externally may result in progression along the KFMASH univariancy (Fig. 7), resulting in changes in compositions of ferromagnesian phases, as well as variations in the modal proportions of phases.

The equilibria modeled in this paper constitute the fluid-free, multivariate, KNCFMMASH analogue of the univariant KFMASH reaction shown in Fig. 7. The P–T path in Fig. 2 is analogous to migration along the KFMASH univariancy *after* cordierite has been stabilized. Persistence of the phase assemblage in the multivariate case does not depend on fortuitous variations in T and P required for the univariant system. The present analysis has not addressed the P–T history which led to the initial formation of cordierite, just as movement along the KFMASH univariancy gives little information about the P–T path prior to stabilization of the univariant phase assemblage. The first appearance of cordierite at high grade in the McCullough pelitic gneisses may well have occurred along the prograde path (Part I), as described for the fictive clockwise path in Fig. 7. However, once cordierite was present as a stable phase, variations in its modal abundance were a function of the *subsequent* P–T path. It must be borne in mind that this later path may have had a very different slope from that which originally intersected the cordierite stability field.

Clearly, insofar as comparisons are possible, results presented here are not at odds with the data of Holdaway & Lee (1977). Their data and the present calculations (Fig. 2) both indicate an increase in Fe/(Fe + Mg) for cordierite in equilibrium with biotite, garnet, sillimanite, quartz, and K-feldspar as P and T decrease along a steep, positively sloping P–T path. In addition, the present calculations have provided a means for quantitatively monitoring variations in mode along this path. Holdaway & Lee's data give no information regarding extensive parameters.

Tectonic implications

In Part I it was concluded that spatially and temporally coincident granitic plutonism was a likely cause for Proterozoic high-grade metamorphism of the pelitic gneiss. Decompression resulting from uplift and erosion and/or extensional tectonism may have contributed to the low pressures attained at near-peak temperatures. The steep decompression path in Fig. 2 is evidence that unroofing was an important factor in determining the thermobarometric history of these rocks.

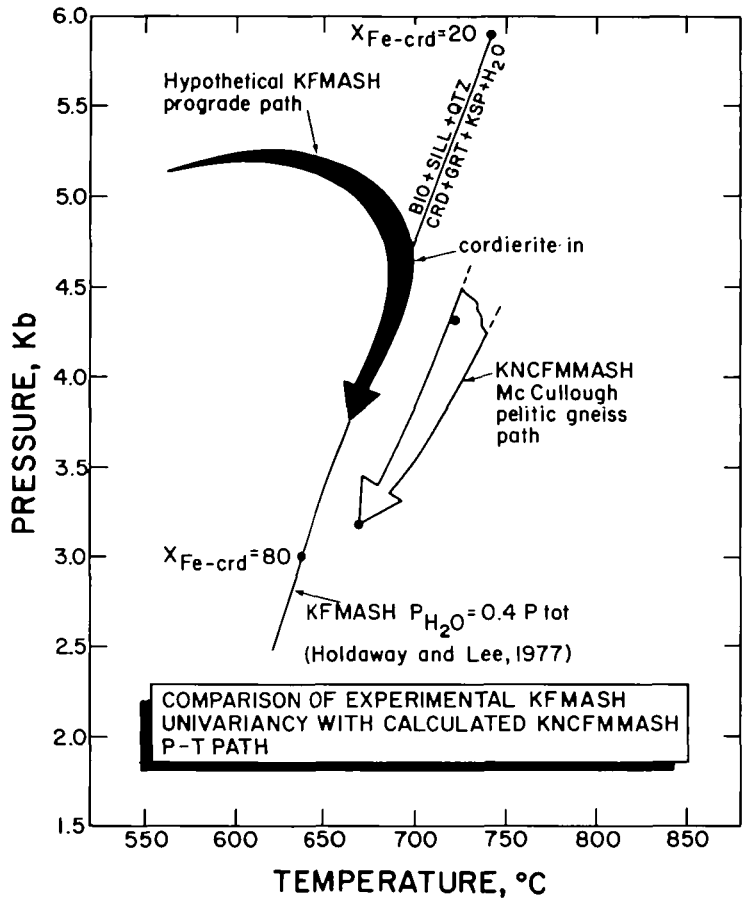

FIG. 7. Comparison of the KFMASH univariancy BIO + SILL + QTZ $\rightleftharpoons$ CRD + GRT + KSP + H_2O after Holdaway & Lee (1977) and the *P–T* path for the McCullough pelitic gneiss. Solid black arrow depicts the hypothetical clockwise *P–T* path in the KFMASH system described in text. Cordierite composition data (labelled dots) are from Holdaway & Lee.

The time-dependent conductive heat transfer models of England & Thompson (1984) suggest that the slope of the *P–T* path calculated here can be explained by an episode of tectonic thickening. Their models predict that relatively low pressures attending near-peak temperatures are favored by isobaric heating followed by erosion in such an event. However, transient thermal gradients induced by conductive heating of tectonically thickened crust cannot alone accommodate granulite-grade low-pressure metamorphism (Thompson & England, 1984). For this reason, high thermal gradients brought about by denudation, as evidenced by the steep *P–T* path recorded in these rocks, must have been significantly enhanced by advective heating from rising plutons.

Bohlen (1987) has shown that medium pressure facies series granulites (kyanite-sillimanite facies series) characteristically exhibit evidence for essentially isobaric cooling paths. He argued that isobaric cooling of these rocks represents the high-pressure culmination of evolution along a counterclockwise *P–T* path in an active magmatic arc setting. Thompson & England (1984) noted that isobaric cooling is not sufficient evidence for magmatic involvement in metamorphism, and suggest that accelerated unroofing of a collision zone by

late stage extensional tectonism can result in isobaric cooling along a clockwise P–T path (Thompson & England, 1984, fig. 7C). In either case, the P–T path segment shown in Fig. 2 for the low-pressure McCullough granulites contrasts sharply with that for higher pressure granulites and indicates that these two classes of high-grade rocks evolve in distinctly different thermal regimes. The retrograde path of the McCullough granulites was strongly influenced by synmetamorphic unroofing, while the retrograde path for kyanite–sillimanite facies series granulites involve minimal erosion, except perhaps during the latest stages.

As shown by Sleep (1979) and Chamberlain (1986), disparate, even diverging P–T paths may occur in metamorphic terranes where metamorphism is synchronous with rapid, large-amplitude folding. Structural evidence for synmetamorphic nappe development has not been recognized in the McCullough complex, but is not precluded by the P–T path shown in Fig. 2.

CONCLUSIONS

Compositional differences between inclusion and matrix mineral assemblages in granulite-grade biotite–cordierite–garnet gneisses exposed in the McCullough Range are the result of a continuous net-transfer reaction. A thermodynamic model based on the approach of Spear (1986) permits reconstruction of variations in both intensive and extensive parameters which accompanied this reaction. Textural evidence and mineral compositions require the model assemblages to be treated as a fluid-absent system open to transfer of H_2O.

The model indicates that the continuous reaction is characterized by the growth of cordierite and K-feldspar, breakdown of biotite, sillimanite, and quartz, an increase in $FeMg_{-1}$ in the ferromagnesian phases, and a decrease in $Al_2R^{2+}_{-1}Si_{-1}$ in biotite. This reaction progressed with decreasing P, decreasing T, and increasing a_{H_2O}. The calculated P–T path slope is approximately 22 b/°C. The magnitude of decompression is subject to significant uncertainty but is on the order of 1 kb with a range of 0·5–3 kb. Decompression during minimal cooling distinguishes these low-pressure granulites from higher pressure granulite terranes which commonly exhibit evidence for isobaric cooling.

Consideration of extensive as well as intensive parameters can facilitate thermodynamic analysis of high variance systems largely closed to mass transfer by reducing the total number of independent factors of state. Linkage of mass balance equations to the Gibbs Method, as suggested by Spear (1986), is a useful formulism for including extensive variables in the analysis of parageneses.

ACKNOWLEDGEMENTS

The author is indebted to J. Lawford Anderson and Warren M. Thomas for making this work possible. Fieldwork and collection of microprobe data were supported by a grant from the U.S. Geological Survey Branch of Central Mineral Resources to Warren M. Thomas. Funding was also provided by NSF grant EAR 86-18285 to J. Lawford Anderson. The manuscript was greatly improved following critical reviews by Edgar Froese and James A. Grant. Frank S. Spear is gratefully acknowledged for several enlightening discussions, and for his critical reading of an earlier version of this work.

REFERENCES

Anderson, G. M., 1976. Error propagation by the Monte Carlo method in geochemical calculations. *Geochim. Cosmochim. Acta* **40**, 1533–8.

Aranovich, L. Y., & Podlesskii, K. K., 1983, The cordierite–garnet–sillimanite–quartz equilibrium: experiments and applications. In: Saxena, S. K. (ed.) *Kinetics and Equilibrium in Mineral Reactions*. New York: Springer-Verlag, 173–98.

Bohlen, S. R., 1987. Pressure–temperature–time paths and a tectonic model for the evolution of granulites. *J. Geol.* **95**, 617–32.

Burnham, C. W., Holloway, J. R., & Davis, N. F., 1969. Thermodynamic properties of water to 1000°C and 10000 bars. *Spec. Paper Geol. Soc. Am.* **132**, 96.

Chamberlain, C. P., 1986. Evidence for the repeated folding of isotherms during regional metamorphism. *J. Petrology* **27**, 63–90.

England, P. C., & Thompson, A. B., 1984. Pressure-temperature-time paths of regional metamorphism I. Heat transfer during the evolution of regions of thickened continental crust. *Ibid.* **24**, 894–928.

Grew, E. S., 1981. Granulite-facies metamorphism at Molodezhnaya Station, east Antarctica. *Ibid.* **22**, 297–336.

Hoffer, E., 1976. The reaction sillimanite + biotite + quartz $\rightleftharpoons$ K-feldspar + H_2O and partial melting in the system K_2O–FeO–MgO–Al_2O_3–SiO_2–H_2O. *Contr. Miner. Petrol.* **55**, 127–30.

Holdaway, M. J., & Lee, S. M., 1977. Fe–Mg cordierite stability in high-grade pelitic rocks based on experimental, theoretical, and natural observations. *Contr. Miner. Petrol.* **63**, 175–98.

Hollister, L. S., 1977. The reaction forming cordierite from garnet, the Khtada Lake metamorphic complex, British Columbia. *Can. Miner.* **15**, 217–29.

Indares, A., & Martignole, J., 1984. Evolution of *P–T* conditions during a high-grade metamorphic event in the Maniwaki area (Grenville Province). *Can. J. Earth Sci.* **21**, 853–63.

Jamieson, R. A., 1984. Low pressure cordierite-bearing migmatites from Kelly's Mountain, Nova Scotia. *Contr. Miner. Petrol.* **86**, 309–20.

Korzhinskii, D. S., 1959. *Physiochemical Basis of the Analysis of the Paragenesis of Minerals*. New York: Consultants Bureau, 142 pp.

Loomis, T. P., 1975. Reaction zoning of garnet. *Contr. Miner. Petrol.* **52**, 285–305.

Martignole, J., & Sisi, J. C., 1981. Cordierite–garnet–H_2O equilibrium: a geological thermometer barometer and water fugacity indicator. *Ibid.* **77**, 38–46.

Reinhardt, E. W., 1968. Phase relations in cordierite-bearing gneisses from the Ganaoque area, Ontario. *Can. J. Earth Sci.* **5**, 455–82.

Rice, J. M., & Ferry, J. M., 1982. Buffering, infiltration, and the control of intensive variables during metamorphism. In: Ferry, J. M. (ed.). *Characterization of Metamorphism through Mineral Equilibria. Min. Soc. Am., Rev. Miner.* **10**, 263–326.

Rumble, D. III, 1982. The role of perfectly mobile components in metamorphism. *Ann. Rev. Earth planet. Sci. Lett.* **10**, 221–31.

Schreurs, J., & Westra, L., 1986. The thermotectonic evolution of a Proterozoic low pressure, granulite dome, West Uusimaa, SW Finland. *Contr. Miner. Petrol.* **93**, 236–50.

Sleep, N. H., 1979. A thermal constraint on the duration of folding with reference to Acadian geology, New England (USA). *J. Geol.* **87**, 583–9.

Spear, F. S., 1986. The Gibbs Method, Duhem's Theorem and *P–T–X*(Fe–Mg–Mn) relations in pelites. *abs. EOS. Trans. Am. Geo-physical Union annual meeting* **67**, 16, 407.

—— Ferry, J. M., and Rumble, D. III, 1982. Analytical formulation of phase equilibria: the Gibb's method. In: Ferry, J. M. (ed.) *Characterization of Metamorphism through Mineral Equilibria. Min. Soc. Am., Rev. Miner.* **10**, 105–52.

—— Rumble, D. III, 1986. Pressure, temperature, and structural evolution of the Orfordville, Belt, west-central New Hampshire. *J. Petrology* **27**, 1071–93.

—— Selverstone, J., 1983. Quantitative *P–T* paths from zoned minerals: theory and tectonic applications. *Contr. Miner. Petrol.* **83**, 348–57.

Thompson, A. B., 1976. Mineral reactions in pelitic rocks: I. Prediction of *P–T–X*(Fe–Mg) phase relations. *Am. J. Sci.* **276**, 401–24.

—— 1983. Fluid-absent metamorphism. *J. geol. Soc. Lond.* **140**, 533–47.

—— England, P. C., 1984. Pressure–temperature–time paths of regional metamorphism II. Their influence and interpretation using mineral assemblages in metamorphic rocks. *J. Petrology* **25**, 929–55.

Thompson, J. B., Jr., 1970. Geochemical reaction and open systems. *Geochim. Cosmochim. Acta* **34**, 529–51.

—— 1982. Composition space: an algebraic and geometric approach. In: Ferry, J. M. (ed.). *Characterization of Metamorphism through Mineral Equilibria. Min. Soc. Am., Rev. Miner.* **10**, 1–31.

—— Laird, J., and Thompson, A. B., 1982. Reactions in amphibolite, greenschist and blueschist. *J. Petrology* **23**, 1–27.

Tracy, R. J., & Dietsch, C. W., 1982. High-temperature retrograde reactions in pelitic gneiss, central Massachusetts. *Can. Miner.* **20**, 425–37.

—— Robinson, P., & Thompson, A. B., 1976. Garnet composition and zoning in the determination of temperature and pressure of metamorphism, central Massachusetts. *Am. Miner.* **61**, 762–75.

Woodsworth, G. J., 1977. Homogenization of zoned garnets from pelitic schists. *Can. Miner.* **15**, 230–42.